ACS EARTH AND SPACE CHEMISTRY

Article

Cite This: ACS Earth Space Chem. 2019, 3, 2197−2206

http://pubs.acs.org/journal/aesccq

Plutonium Retention Mechanisms by Magnetite under Anoxic Conditions: Entrapment versus Sorption

Thomas Dumas,[†,‡,⊥] David Fellhauer,[§,∥] Dieter Schild,[§] Xavier Gaona,[§] Marcus Altmaier,[§] and Andreas C. Scheinost*[,†,‡]

[†]The Rossendorf Beamline at ESRF, Grenoble, France

[‡]HZDR Inst. of Resource Ecology, Dresden, Germany

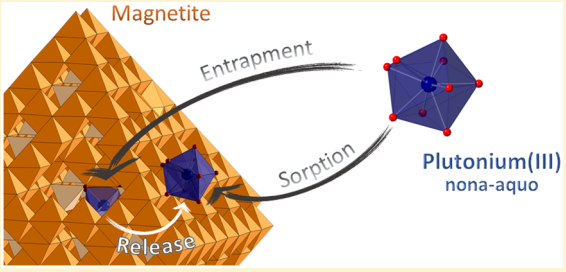
[§]KIT Inst. for Nuclear Waste Disposal, Karlsruhe, Germany

[∥]JRC Karlsruhe, Karlsruhe, Germany

[⊥]French Nuclear and Alternative Energies Commission CEA Nuclear Energy Division—CEA Marcoule Research, Department of Mining and Fuel Recycling ProCesses (DMRC), Site de Marcoule, BP17171, 30207 Bagnols sur Cèze, France

Supporting Information

ABSTRACT: The reliable prediction of possible plutonium migration into the geological environment is crucial for the safety assessment of radioactive waste repositories. Fe(II)-bearing corrosion products like magnetite, which form on the surface of steel waste containers, can effectively contribute to the retardation of the potential radionuclide release by sorption and redox reactions, eventually followed by formation of secondary precipitates. A retardation process even more efficient—especially when considering the required long time scales for nuclear waste reposition—is structural incorporation by magnetite, as has been demonstrated for Tc and U. Here we show that this mechanism might not be as relevant for Pu retention: after a rapid reduction of Pu(V) to Pu(III) in acidic Fe(II)/Fe(III) solution, base-induced magnetite precipitation ($pH_{exp} \approx 12.5$) leads only to a partial (~50%) incorporation, while the other half remains at the surface by forming tridentate sorption complexes. Neither solid nor sorbed Pu(IV) species were observed in the starting solution and after precipitation. With Fe(II)-enforced recrystallization at pH_{exp} = 6.5, a process potentially mimicking long-term, thermodynamically controlled aging, the equilibrium between both Pu species is even further shifted toward the sorption complex. A detailed analysis of the incorporated species by Pu L_{III}-edge X-ray absorption fine-structure (XAFS) spectroscopy shows a pyrochlore-like coordination environment (split 8-fold oxygen coordination shell with Pu−O distances of 2.22 and 2.45 Å and an edge-sharing linkage to Fe-octahedra with Pu−Fe distances of 3.68 Å), which is embedded in the magnetite matrix (Pu−Fe distances of 3.93, 5.17, and 5.47 Å). This suggests that the reason for the partial incorporation is the structural incompatibility of the large Pu(III) ion for the octahedral Fe site in magnetite. The adoption of a pyrochlore-like local environment within the magnetite long-range structure might be induced by the rapid coprecipitation rather than being a thermodynamically stable state (kinetic entrapment).



KEYWORDS: *Plutonium, magnetite, redox, XAFS spectroscopy, radioactive waste*

Downloaded via LOS ALAMOS NATL LABORATORY on November 1, 2024 at 21:05:20 (UTC).
See https://pubs.acs.org/sharingguidelines for options on how to legitimately share published articles.

INTRODUCTION

As the major chemical and radiotoxic transuranium element in civil and military nuclear waste, plutonium has to be considered as a major issue for the long-term safety of nuclear waste repositories. Unlike the lanthanides, and more similar to its early actinide neighbors uranium and neptunium, plutonium can occur in several oxidation states within the water stability field, including III, IV, V, and VI.[1] Given the complexity to work with Pu, relatively few studies have been conducted to elucidate potential links between Pu oxidation state, its association with minerals in the sediments, and the desorption or migration behavior. In lysimeter experiments with natural sediments,[2−4] all oxidation states were observed in the aqueous phase, while Pu(IV) prevailed in association with the solid phase and increased with time. Pu solubility increased under subsequent oxidative conditions, presumably through partial oxidation of Pu(IV) to more soluble Pu(V), and/or through lowering the pH by one unit in line with the equilibrium solubility of PuO_2. After sorption to natural tuff, Pu(V) and Pu(VI) was found to be associated with manganese oxide and clay minerals, but not with iron oxide.[5] At the Nevada Test Site (USA) and at the Mayak Production Association (Russian Federation), Pu was associated with aluminosilicate and iron (hydr)oxide colloids, respectively, thereby undergoing colloid-facilitated transport.[6,7] Processes

Received: May 24, 2019
Revised: July 19, 2019
Accepted: July 21, 2019
Published: July 21, 2019

© 2019 American Chemical Society

DOI: 10.1021/acsearthspacechem.9b00147
ACS Earth Space Chem. 2019, 3, 2197−2206

influencing Pu migration and uptake by biota, including complexation and redox reactions of Pu with humic substances, peptides, and proteins, with bacteria and with a range of minerals, have been predominately investigated under oxic conditions.[8−14] In the case of the deep underground repositories foreseen by several countries for disposal of nuclear waste, however, anoxic conditions will develop soon after closure of the mine shafts. In addition, radiolytic water dissociation under near-field conditions will produce hydrogen gas, further lowering the redox potential.[15] Under such conditions, the first technical barrier consisting of stainless-steel casks will corrode over the geological time scales to be considered. Depending on the technical backfill material (clays like bentonite), the natural bedrock (e.g., clay, granite, or salt), and the nature of the eventually penetrating groundwater, a range of Fe(II)-bearing minerals may form during the corrosion processes, including oxides like magnetite (Fe_3O_4), sulfides like mackinawite (FeS), and (hydroxo) carbonates like siderite ($FeCO_3$) and chukanovite ($Fe_2(OH)_2(CO_3)$), as well as Fe-rich clays like nontronite.[16−19] The low redox potential along with the catalytic effect of these Fe(II)-bearing minerals has been shown to greatly reduce the mobility of redox-reactive actinides (U, Np) and fission products (Se, Tc) by sorption and reduction processes producing solid compounds with very low solubility like $U^{IV}O_2$,[20−24] $Np^{IV}O_2$,[25−27] FeSe,[28−30] and $Tc^{IV}O_2$.[23,31,32] While formation of PuO_2 with similarly low solubility has also been observed during mineral sorption reactions under both oxic and anoxic conditions,[33−35] Pu may also be further reduced to the oxidation state III, where it occurs as aquo ion with high solubility in acidic to weakly alkaline solutions. Note the similar geochemical behavior of Pu(III) with its next actinide neighbors, Am and Cm, which are prevalently trivalent. Formation of Pu(III) by magnetite has in fact been confirmed by Kirsch et al. under anoxic conditions similar to those expected for deep underground repositories.[36] A very stable Pu(III) surface complex was identified, where mononuclear Pu(III) atoms are linked via three oxygen atoms to three edge-sharing FeO_6-octahedra at the magnetite {111} faces. This surface complex has a high affinity toward the magnetite surface as expressed by Pu concentrations below 10^{-9} M (i.e., the detection limit of liquid scintillation counting for ^{242}Pu).

The release of Fe(II) from hydrogen-driven steel corrosion and subsequent precipitation of magnetite may create a highly dynamic system where one could envision that Pu is incorporated by magnetite following either a coprecipitation process or by overgrowth of an already existing magnetite surface with adsorbed Pu. Such a process has been observed, for instance, for Tc(IV) and Sn(IV), two cations with ionic radii (0.65 and 0.69 Å, respectively) similar to those of Fe(II) or Fe(III) (0.78 and 0.65 Å, respectively), which therefore can easily replace Fe in octahedral sites.[32,37,38] More surprisingly, from a crystal-chemical point of view, this has also been demonstrated for the larger actinide U.[39−41] In this case, U is preferentially incorporated in its pentavalent oxidation state, by adopting an uranate-type local structure characterized by relaxation of the multiply bonded "-yl" oxygen ligands.

The ionic radius of trivalent Pu (1.00 Å), along with that of Am (0.975 Å) and Cm (0.95 Å), however, seems to be too large to be hosted by the octahedral site of Fe with average oxidation state of 2.5 and an expected average ionic radius of 0.713 Å ((0.645 + 0.78)/2). Nevertheless, a significant body of work shows incorporation of early trivalent lanthanides, which have ionic radii similar to those of the early actinides, by magnetite through a variety of synthesis procedures including bacterial processes. While none of these studies investigated the short-range structure around the lanthanide dopant, the long-range magnetite structure as determined by X-ray diffraction (XRD) was conserved for up to a few percent of dopant.[42−48]

To the best of our knowledge, there are only two recent studies trying to decipher the local structure of Sm- and Am-doped magnetite by Sm and Am L_{III}-edge XAFS spectroscopy.[49,50] In both cases doping was successful, while the local structure was in disagreement with a simple Sm/Am-for-Fe substitution at either the octahedral or (even less likely) the tetrahedral site in magnetite. For Am, the short-range order probed by EXAFS showed a 7-fold coordination of Am and Am−Fe distances largely incompatible with the Fe Oh site in magnetite for a fresh sample at pH 5.7, while in a sample aged for two years at pH 12.5, Am was 6-fold coordinated more commensurate with the Fe Oh site. Beyond the coordination sphere, however, only 1.5 Fe at 3.40 Å were found, contradicting the substitution into the Fe Oh site, but rather suggesting an alternative local environment. A definitive elucidation was not successful, most likely because of high structural disorder and/or the presence of several local environments, which because of the intrinsically poor resolution of EXAFS (0.1 to 0.2 Å depending on available k-range) are often impossible to discriminate.

The intention of our study was therefore to conduct plutonium/magnetite coprecipitation experiments under anoxic conditions in order to verify if incorporation may also occur for the redox-susceptible Pu. We used Pu(V) and Pu(III) as initial oxidation states and followed their oxidation state and local structure during coprecipitation with a mixed Fe(II) and Fe(III) solution using XAFS spectroscopy. In contrast to the previous Am studies, we analyzed the spectroscopic data also with advanced chemometric tools in order to enhance resolution and to discriminate the spectral signal from eventually coexisting multiple species. The fresh magnetite coprecipitates were further subjected to Fe(II)-enforced recrystallization, a process, which has been shown to increase structural incorporation of size-compatible cations as e.g. Ni in goethite,[51] and potentially mimics long-term, more thermodynamically controlled aging.[52−55]

EXPERIMENTAL SECTION

Warning. ^{242}Pu is a highly radiotoxic α-emitter, which must be handled in dedicated laboratory facilities. Its possession and use is subject to strict statutory controls.

General Synthesis and Analysis Conditions. All sample manipulations, including mineral synthesis, washing, preparation of samples for XAS, and UV−vis measurements, were carried out under anoxic conditions in argon-atmosphere glove-boxes with <10 ppmv O_2. Samples for XAFS analysis were stored and transported to the synchrotron facility under LN_2 and then measured at 15 K under He atmosphere in a closed-cycle cryostat (CryoVac). Wet chemistry experiments were carried out at room temperature using deionized (18.2MΩ Milli-Q), degassed (O_2 and CO_2 free) water for all purposes.

Preparation of Pu Stock Solutions. The employed Pu had an isotope composition of 99.4 wt % ^{242}Pu, 0.58 wt % ^{239}Pu, 0.005 wt % ^{238}Pu, and 0.005 wt % ^{241}Pu. Solutions of 1.1 mM Pu(V) and 1.8 mM Pu(III) were prepared electrolytically

DOI: 10.1021/acsearthspacechem.9b00147
ACS Earth Space Chem. 2019, 3, 2197−2206

in 0.5 M NaCl with pH_{exp} 3, and in 0.1 M $NaClO_4$ with pH_{exp} 2, respectively. UV−vis spectroscopy (Figure 1) confirmed the

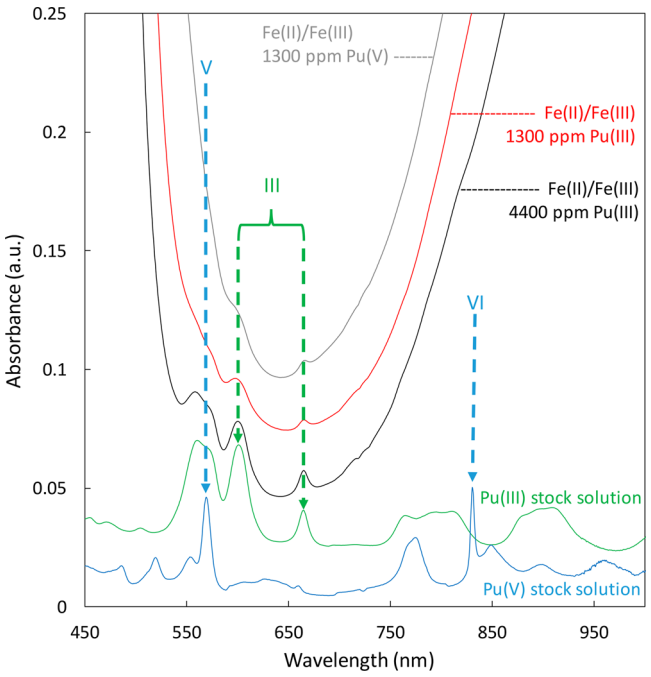


Figure 1. UV−vis spectra of Pu(III) and Pu(V) stock solutions and of the mixed Fe(II)/Fe(III)/Pu solutions before coprecipitation. The two most prominent absorption bands of Pu(III) are marked with green hatched lines, the bands of Pu(V) and Pu(VI) are marked in blue hatched lines. For clarity, the spectra of the Pu(V) and Pu(III) stock solution were rescaled by a factor of 2 and 0.5, respectively, to account for the different molar absorption coefficients. In addition, the spectra have been vertically shifted by 0, 0.02, 0, 0.005, and 0.02 absorption units from bottom to top for better readability. Note the strongly curved background of the mixed solutions due to the broad absorption bands of Fe(II) and Fe(III) species below 550 and above 750 nm.

prevalence of the intended oxidation states, and liquid scintillation counting (LSC) conducted before and after 10 kDa ultrafiltration confirmed the absence of significant amounts of PuO_2 colloids in the stock solutions. Note that the relatively strong Pu(VI) peak in the spectrum of the Pu(V) stock solution corresponds to less than 10% Pu(VI) impurity due to the much higher molar absorption coefficient of Pu(VI) in relation to Pu(V).

Pu-Magnetite Coprecipitation. Experiments were conducted with either Pu(V) or Pu(III). Five milliliters of Fe(II)/Fe(III) solutions were prepared by mixing 2.5 mL of 0.8 mol·L^{-1} $FeCl_2$ solution with 2.5 mL of 1.6 mol·L^{-1} $FeCl_3$ solution and adjusted to pH_{exp} 1.5. Pu(V) or (III) stock solutions were then added to the iron solutions (1.8 mL for Pu(V) and 1.35 or 4.72 mL for Pu(III)). UV−vis spectroscopy showed a rapid reduction of Pu(V) to Pu(III) for the first sample (Figure 1), whereas the oxidation state in the two Pu(III) samples remained stable. Further experiments were hence conducted only with the two Pu(III) samples, labeled **Pu-Mag-1300** and **Pu-Mag-4400** with the numbers referring to the target Pu concentration in each sample in μg/g (ppm). Pu coprecipitation with *in situ* formed magnetite was induced by rapidly pouring the Fe/Pu solutions into 3.3 mL of a 6 M NaOH solution. pH_{exp} and pe were determined in the black suspensions after 5 min when stable potentials were reached. Pu-Mag-1300 had a pH_{exp} of 12.4 and a pe of −11.1, while Pu-Mag-4400 had a pH_{exp} of 12.5 and a pe of −11.3. After centrifugation, a 1 mL aliquot of the supernatant was separated for further wet chemical analysis. The bottom slurry of magnetite was washed three times with 5 mL of degassed water, and after centrifugation, the resulting wet paste was isolated for further XRD and XAFS analyses.

Fe-Enforced Recrystallization Procedure. We adapted a procedure from Boland et al.[52] to enhance recrystallization of the iron oxide phases through concomitant Fe(II)/Fe(III) electron exchange, oxide growth, and reductive dissolution.[53−56] An aliquot equivalent to ∼225 mg of dry Pu-Mag-1300 and Pu-Mag-4400 samples was added under stirring into 100 mL of a solution containing 1 mM Fe(II) and buffered at pH_{exp} 6.5 by 50 mM MES buffer (2-(*N*-morpholino)-ethanesulfonic acid). After 5 days of reaction, the solid samples were centrifuged and isolated as wet paste for further XAFS and XRD analyses (samples **Pu-Mag-1300-rec** and **Pu-Mag-4400-rec**).

Supernatant Characterization. The Pu content in the supernatant was measured by LSC. In all four samples, both before and after aging, Pu concentration in the supernatant was below the LSC detection limit ($<10^{-9}$ mol L^{-1}), i.e., most Pu was associated with the solid phase.

Magnetite Characterization. XRD patterns (Cu source) of Pu-Mag-1300, Pu-Mag-4400, Pu-Mag-1300a, and Pu-Mag-4400a demonstrate the phase identity and purity by showing only the 220, 311, 400, 511, and 440 reflections of the magnetite cubic cell (*Fd*3*m*) (Figure 2). The broadening of the diffraction bands as evaluated by the Debye−Scherrer equation provides an average crystallite size of 10 nm, which we could not confirm by TEM, but which should be—according to

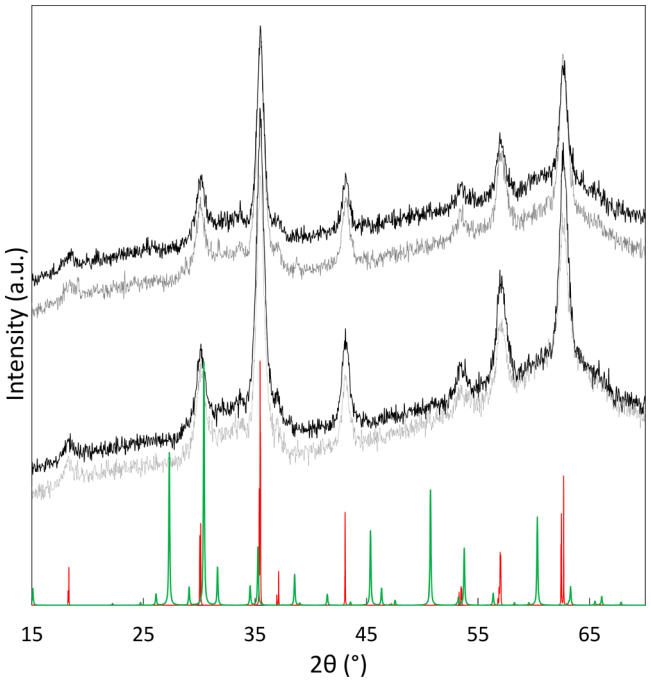


Figure 2. Powder-XRD for samples Pu-Mag-1300, Pu-Mag-1300-rec, Pu-Mag-4400, and Pu-Mag-4400-rec (from top to bottom) and calculated powder pattern from Wright et al.[60] for magnetite (red line) and for the europium pyrochlore-type structure from Chtoun et al.[61] (green line).

DOI: 10.1021/acsearthspacechem.9b00147
ACS Earth Space Chem. 2019, 3, 2197−2206

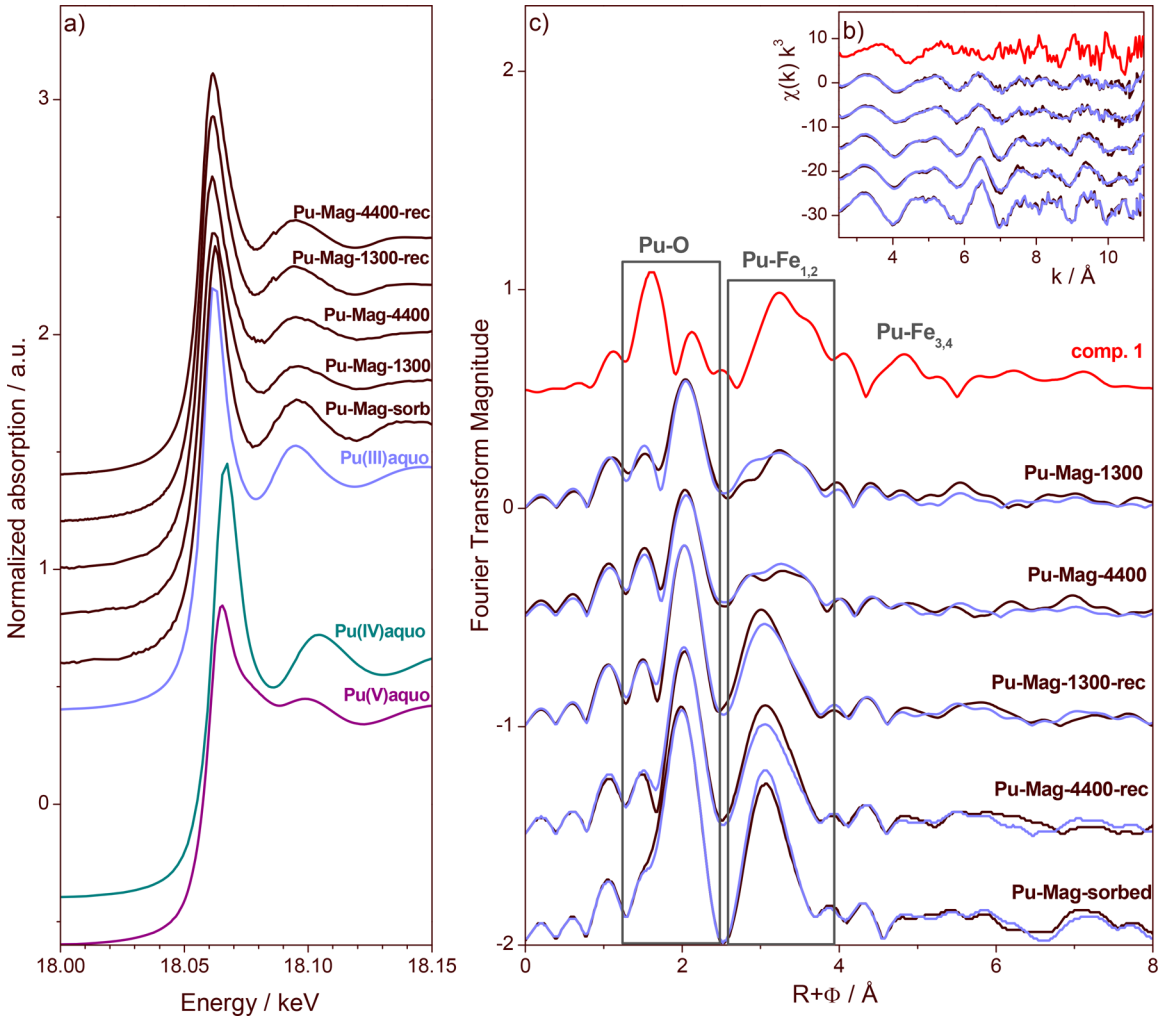


Figure 3. Pu L_{III} edge XAFS spectra of magnetite coprecipitation samples and selected references from Kirsch et al.[36] (a) XANES spectra, (b) k^3-weighted EXAFS spectra, (c) corresponding Fourier transform magnitudes. For b) and c), black lines are experimental data, and blue lines are ITFA-derived reproductions by two components. Using Pu-Mag-sorb (bottom) as one end-member component, the second end-member component (comp. 1) was extracted from the full data set (see text).

previous work where both methods were available—in line with TEM-derived particle diameters of magnetite.[57,58] The Fe(II)/Fe_{tot} ratio in the two nonaged magnetite samples was determined by dissolving the solid samples and then determining the Fe(II) concentration spectrophotometrically[59] in ultrafiltrated (10 kDa) aliquots before (= structural Fe(II)) and after Fe reduction with NH_2OH-HCl (= structural total Fe). The structural Fe(II)/Fe_{tot} ratios of 0.32 (Pu-Mag-1300) and 0.30 (Pu-Mag-4400) were close to the ideal ratio of stoichiometric magnetite (0.33).

X-ray Photoelectron Spectroscopy (XPS). A VersaProbe II (ULVAC-PHI) was used with monochromatized Al Kα radiation (1486.7 eV). Calibration of the binding energy scale of the spectrometer was performed using pure metals (monochromatic Al K_α: Cu $2p_{3/2}$ at 932.62 eV, Au $4f_{7/2}$ at 83.96 eV).[62] Binding energies of elemental lines of the samples are charge referenced to O 1s (oxide) at 530.0 eV. The background pressure in the analysis chamber was about 7×10^{-8} Pa. Samples were prepared by pressing the wet paste from a 2 mL centrifuge tube onto indium foil and then transferred with a vacuum vessel (PHI model V5000-K) from the glovebox into the XPS entry chamber, where pumping overnight removed associated water.

X-ray Absorption Fine-Structure (XAFS) Spectroscopy. XAFS spectra were collected at The Rossendorf Beamline at the European Synchrotron Radiation Facility (ESRF, Grenoble). Its experimental station is a dedicated α-laboratory to measure actinides in double confinement sample holders. The energy of the X-ray beam was tuned by a double-crystal monochromator operating in channel-cut mode using a Si(111) crystal pair. Two platinum-coated Si mirrors before and after the monochromator were used to collimate the beam into the monochromator and to reject higher harmonics. Pu L_3-edge spectra were collected in fluorescence mode using a 13-element energy-dispersive solid-state Ge detector (Canberra) together with a digital signal processing unit (XIA XMap). Spectra were collected at 15 K using a closed cycle He cryostat (CryoVac). Energy calibration was performed using the zero crossing of the second derivative of the K-edge of metallic Zr (17998 eV) measured simultaneously to the sample scans. Dead time correction of the fluorescence signal, energy calibration, and the averaging of the individual scans were performed with the software package SixPack.[63] Normalization, transformation from energy into k-space, subtraction of a spline background, and shell fits were performed with WinXAS following standard procedures.[64] All fits were carried

DOI: 10.1021/acsearthspacechem.9b00147
ACS Earth Space Chem. 2019, 3, 2197−2206

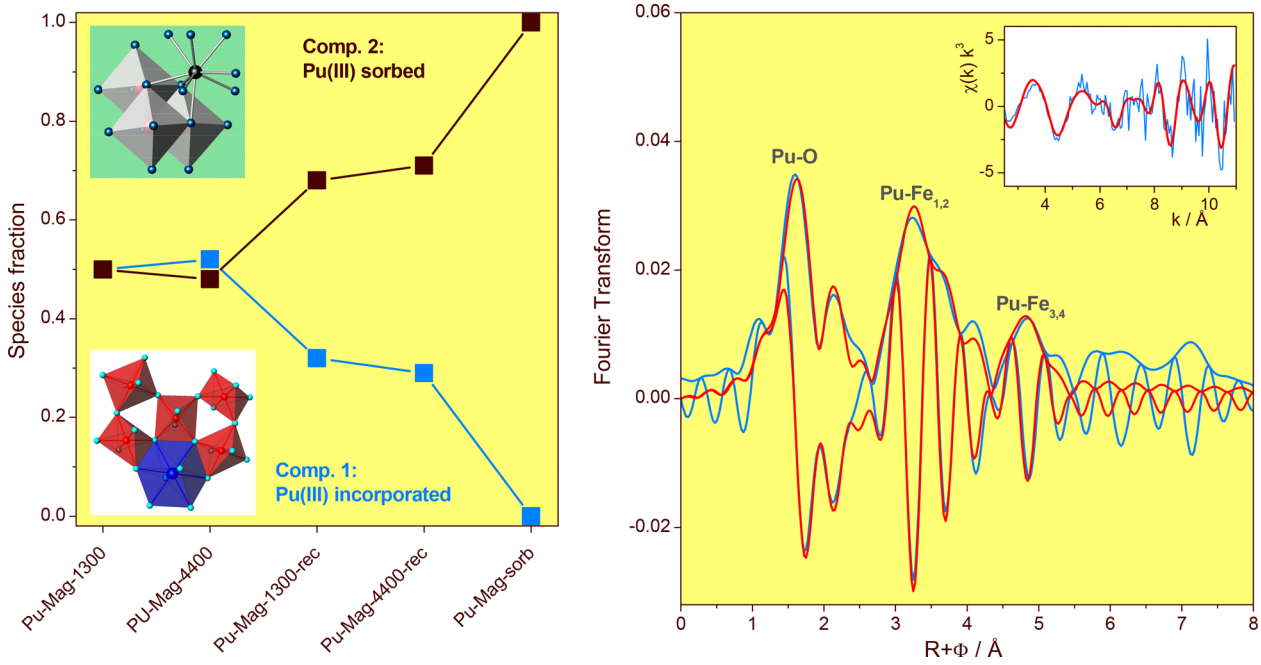


Figure 4. Left: ITFA-derived relative concentrations of components 1 and 2 in each sample. Component 1 corresponds to Pu(III) incorporated by magnetite. Component 2 corresponds to the previously determined Pu(III) sorption complex on magnetite. Right: EXAFS shell fit of component 1 (experimental data, blue lines; best-fit, red line) shown as Fourier transform magnitude and imaginary part, as well as k^3-weighted EXAFS spectra (insert).

out in *R*-space (1 to 5 Å) of k^3-weighted spectra using theoretical backscattering amplitudes and phase shifts calculated with FEFF 8.2[65] on clusters (R_{max} = 8 Å) derived from magnetite[60] and pyrochlore[61] structures, placing Pu into the central six-coordinated Fe and eight-coordinated lanthanide position, respectively. The Debye−Waller factor was restricted to float between 0.002 and 0.015 $Å^{-1}$. Furthermore, spectra were analyzed by iterative transformation factor analysis (ITFA).[66]

RESULTS AND DISCUSSION

The initial aim of this study was to investigate the potential uptake of Pu(III) and Pu(V) by magnetite during coprecipitation. No matter if the starting solution contained Pu(III) or Pu(V), however, a final Pu oxidation state of III was established within less than a minute at $pH_{exp} \approx 1.5$, after mixing with the Fe(II)−Fe(III) solution (Figure 1). Therefore, Pu(V) was reduced directly to Pu(III) without forming a stable Pu(IV) intermediate, and the reduction was far too rapid for even a kinetically controlled incorporation of Pu(V) during formation of magnetite under strongly reducing conditions. By raising the pH to about 12.5 to induce magnetite precipitation, the Pu concentration dropped below the LSC detection limit of 10^{-9} M (corresponding to a solid liquid distribution ratio, log K_d, > 5.5) suggesting either an efficient retention process associated with the magnetite precipitation or a rapid Pu(III) precipitation through hydrolysis.[67,68] After the 5-day Fe-enforced recrystallization process, the Pu concentration remained below the LSC detection limit suggesting at a first glance no change of the retention mechanism.

In order to investigate the Pu oxidation state and the local structure in the fresh and recrystallized magnetite samples, we conducted Pu L_{III}-edge XAFS spectroscopy (Figure 3). The X-ray absorption near-edge structure (XANES) spectra of all samples show a white line at 18063 eV well aligned in energy and shape with those of aqueous Pu(III) and with Pu(III) sorbed to magnetite taken from ref 36 (Figure 3a). The white lines of aqueous Pu(IV) and Pu(V) reference samples[69] occur at significantly higher energies, and that of Pu(V) shows furthermore the typical shape characteristic of the trans-dioxo(-yl) configuration on the right-wing side of the white line. Therefore, the trivalent oxidation state initially present in solution is well preserved after coprecipitation. Linear combination fitting of the spectra confirmed that eventual contributions from oxidation states IV and V are absent or below 2% (not shown). Formation of PuO_2 associated with the solid phase can further be excluded by XPS since the corresponding satellite peak around 432 eV is absent, and only the $4f_{7/2}$ peak at 425.2 eV in close agreement with Pu(III) reference samples is present (Supporting Information).

The extended X-ray absorption fine-structure (EXAFS) spectra and their Fourier transform magnitudes (FTM), which represent pseudoradial distribution functions of the atomic neighbors of Pu, with the distances deviating by about 0.4 Å due to the phase shift Φ, are shown in Figure 3b,c, respectively. The two spectra collected after the recrystallization procedure (Pu-Mag-1300-rec and Pu-Mag-4400-rec) are very similar to each other and resemble that of the Pu(III) magnetite sorption sample, suggesting that Pu(III) prevails as the tridentate sorption complex previously identified.[36] The spectra of the two fresh coprecipitation samples (Pu-Mag-1300 and Pu-Mag-4400), however, have weaker Pu−O and Pu−$Fe_{1,2}$ FTM peaks in comparison to the sorption complex, suggesting a more distorted local environment or the presence of several Pu species with differing local structures.

In order to determine the short-range structure of the fresh coprecipitation samples, we attempted shell fitting based on the magnetite structure, where we replaced Fe in octahedral position by Pu. As expected from the large size difference between Fe and Pu(III) cations, the spectra of Pu-Mag-1300

DOI: 10.1021/acsearthspacechem.9b00147
ACS Earth Space Chem. 2019, 3, 2197−2206

and Pu-Mag-4400 could not be fit with this approach. Several other fit approaches using single or split Pu−O and Pu−Fe shells did not provide satisfactory results because of (1) poor spectral reproduction (approach 1 in Table SI-1, Figure SI-2 top), (2) oxygen coordination numbers of >12 and hence far higher than those expected for octahedral magnetite positions (6) or the typical tricapped prismatic coordination of trivalent lanthanide and actinide aquo-complexes (9) (approaches 2 and 3 in Table SI-1, Figure SI-2 center and bottom), and (3) Debye−Waller factors hitting the upper and lower limit of a physically reasonable range (0.002 and 0.015 Å^2). Furthermore, wavelet analysis[70] of the Fourier peak around 3 Å clearly revealed the presence of backscattering from a medium-heavy atom like Fe, and not from a heavy atom like Pu, excluding, for instance, the formation of Pu_2O_3 with Pu−Pu distances of 3.62 and 4.16 Å.[71] Therefore, we had to assume the existence of two or more coexisting Pu species, which cannot be resolved by shell fitting because of the limited resolution (≥0.17 Å at the given k range of 2 to 11 Å^{-1}). In such cases, iterative transformation factor analysis (ITFA) has shown to be a valuable approach to determine the number of spectral components (often commensurate to number of species) and to extract the spectra of the pure end-member species.[32,66] In fact, the spectra of all four precipitation samples are well reproduced by only two components (compare blue and black traces in Figure 3b,c), suggesting that two structurally distinguishable Pu species are present in these samples. Furthermore, adding the spectrum of Pu(III) sorbed to magnetite (Pu-Mag-sorb) to the other four spectra did not increase the number of significant components, which indicates that this species is indeed one of the two components, as already suggested by the spectral similarity with the two recrystallized samples. Using this information, we could extract the spectrum of the other, unknown component ("comp. 1" shown as top red trace in Figure 3b,c) and calculate the fractions of the two species in each sample spectrum (Figure 4 left). Surprisingly, the fresh precipitates contain already 50 ± 5% of component 2, the Pu(III) sorption complex, and its percentage even increases with the recrystallization procedure to about 70 ± 5%. Therefore, even the spectra of the fresh precipitates contain only 50 ± 5% contribution from component 1, which explains the failure of shell fitting for solving its structure. When using the ITFA-extracted spectrum of component 1, however, we could fit all shells out to a distance of 5.5 Å ($R + \Phi$), well reproducing the EXAFS chi function as well as magnitude and imaginary parts of the Fourier transform (Figure 4 right). The fit parameters are given in Table 1.

In component 1, Pu(III) coordinates to about eight oxygen atoms at two different distances, 2.22 and 2.45 Å. Not surprisingly because of the size mismatch between Pu(III) and Fe(II,III), this coordination is very different from the six-coordinated Fe site in magnetite with a much smaller Fe−O distance of 2.06 Å. The larger distance of 2.45 Å is identical to that of the Pu(III) aquo ion and sorption complexes of Pu or Am with 9-fold oxygen coordination.[36,72] The split shell with an additional shorter Pu−O distance suggests, however, a coordination environment much more distorted than in the trigonal tricapped prism arrangement typical for trivalent lanthanides and actinides in aqueous environment, where the variation of bond distances is commonly too small to be resolved by EXAFS.

Table 1. EXAFS Shell Fit Parameters for Component 1 along with the Crystallographic Data for the Fe-Occupied Oh Site in Magnetite and the Local Structure of Component 2 (Sorbed Pu(III)) Taken from Kirsch et al.[36]

	component 1: incorporated Pu(III)[c]			magnetite Oh site #		component 2: sorbed Pu(III)	
paths	CN	R/Å	σ^2/Å^2[a]	CN	R/Å	CN	R/Å
Pu−O_1	4.5	2.22	0.0089[a]	6	2.06		
Pu−O_2	3.8	2.45	0.0089[a]			9	2.45
Pu−Fe_1	2.7	3.68	0.0032[b]	6	2.95	3	3.54
Pu−Fe_2	1.9	3.93	0.0032[b]	6	3.46	3	4.20
Pu−Fe_3	12.0[b]	5.17	0.0150[c]	12	5.11		
Pu−Fe_4	8.0[b]	5.47	0.0150[c]	8	5.42		

[a]Superscripts a, b, c, and d indicate correlated parameters. [b]Coordination numbers fixed to crystallographic values during shell fit. [c]ΔE_0 = 8.4 eV, χ_{res} = 11.1%.

Typical oxide structures capable of hosting large (∼1.00 Å) trivalent lanthanide and actinide cations alongside much smaller transition metal cations are pyrochlores and perovskites.[73] In perovskites with the general formula ABO_3, the large cation site A is coordinated to 12 oxygen atoms, which significantly deviates from the observed 8-fold coordination for Pu. In pyrochlores with the general formula $A_2B_2O_7$, however, the large A cation is coordinated to eight oxygen atoms, well matching the fit value (Table 1). Furthermore, in most pyrochlores the A site typically deviates from the perfect cubic coordination, causing a split coordination shell.[61,74] For instance, in a pyrochlore with the trivalent cations Eu, Fe, and Ti, hence similar in diameter to those in our system, Eu(III) is coordinated to eight oxygen atoms at 2.20 and 2.48 Å, distances well in line with those in component 1 (structure in lower left corner of Figure 4 left).[61] The shortest fitted Pu−Fe_1 distance of 3.68 Å corresponds also fairly well with the shortest Eu−Fe distance of 3.60 Å, arising from the edge-sharing linkage between Eu-hosting polyhedra and the nearest Fe-hosting octahedra in pyrochlore. The next shell of Fe atoms (Pu−Fe_2) occurs at a distance of 3.93 Å, which suggests that their octahedra are linked to the actinide polyhedra through corners with a strongly bent Pu−O−Fe axis. Finally, the fitted two long Pu−Fe distances of 5.17 and 5.47 Å do not occur in the pyrochlore structure; they correspond instead reasonably well (only 0.05 to 0.06 Å longer) with Fe−Fe distances in magnetite and are well fit with corresponding coordination numbers of 12 and 8, respectively (Table 1). The absence of the longer-range order of pyrochlore contradict that a separate pyrochlore phase trapped Pu (note that the small amount of this phase may not be detectable by XRD). Based on the fitted shell distances and coordination numbers, the structure of component 1 can be conceptualized as Pu(III) entrapped in magnetite by adopting a pyrochlore-like structure with a radius of less than 4 Å, which is embedded in the magnetite structure seen beyond 5 Å from the Pu centers.

This experimental data is in clear contradiction to the result of a recent quantum mechanical approach, where structural incorporation into the Oh site of magnetite was predicted.[75] Furthermore, it also does not confirm a postulated 6-fold coordination for Am in magnetite after 2 years of aging at pH ≈ 12,[50] where shell fitting might have been biased by a mix of sorbed and occluded Am species similar to our results before separating their spectral contributions with ITFA. It is well in

DOI: 10.1021/acsearthspacechem.9b00147
ACS Earth Space Chem. 2019, 3, 2197−2206

line, however, with Sm(III) in Sm-doped magnetite being in 8-fold coordination.[49] In this study, unfortunately only very short Sm L-edge EXAFS spectra could be collected due to the following Fe K-edge (up to 8.5 $Å^{-1}$), inhibiting analysis of atom neighbors beyond the first coordination sphere.

CONCLUSION

Our results show that under the given experimental conditions, Pu(V) in a mixed solution of Fe(II) and Fe(III) under anoxic conditions is rapidly reduced to Pu(III), confirming the relevance of this oxidation state previously suggested by thermodynamic data and experiments.[36] The base-induced precipitation product is pure magnetite, which partitions Pu(III) partly by structural incorporation, partly by surface complexation. In the fresh precipitate, both retention mechanisms occur in about equal fractions and are independent of the Pu loading; after the Fe-enforced recrystallization, the sorption complex prevails (about 2/3 versus 1/3 incorporation), again independent of Pu loading. Therefore, in the studied Pu and Fe concentration range, the processes are controlled by the magnetite nucleation, crystallization, and recrystallization mechanisms and kinetics, and not by Pu(III)-dependent parameters.

In all four samples, the calculated retention coefficient for Pu, log K_d, is larger than 5.5, testimony of the strong Pu retention by both mechanisms at two pH values (12.5 for the fresh, 6.5 for the recrystallized samples). Nevertheless, structural incorporation into magnetite, a phase that is stable across a relatively wide geochemical parameter field, may provide a better protection against Pu-remobilization in the case of changing groundwater chemistry, like increasing Eh or decreasing pH, in comparison to sorption at the magnetite surface as has been demonstrated, for instance, for Tc(IV).[76,77] Therefore, the question whether or not the entrapped Pu species represents a thermodynamically stable phase is of substantial interest. In nature, lanthanides are hosted prevalently by minerals with pyrochlore or perovskite structures, where eight- to twelve-coordinated sites offer more space for their large ionic radii than octahedral sites.[73,78] Pyrochlores are also considered as stable waste forms for actinide and lanthanide radionuclides because of the structure's high tolerance of accommodating defects and disorder, including those induced by heavy internal alpha irradiation.[74,79,80] Here, however, we have no evidence for the formation of such a separate phase, but for the formation of small clusters with 8 Å diameter embedded in the magnetite structure, suggesting that the incorporation of Pu(III) into magnetite can only be achieved by a substantial restructuring of the local environment, which may cause structural strain and subsequent expulsion of Pu from the structure. The increase of the sorbed Pu fraction after recrystallization points into this direction. Plutonium uptake into the structure would then be a kinetically driven process (kinetic entrapment), followed by thermodynamically driven expulsion from the structure. While this process provides an intriguing explanation of our observations, we have no proper proof for this since we also changed the pH during the recrystallization from 12.5 to 6.5 to better mimic long-term conditions in the nuclear waste repository.[81] Therefore, we cannot exclude that also the pH and $[Fe^{II}]$ changes in the recrystallization experiment enhanced the solid/liquid ion exchange and Fe(II) and Pu(III) solubility, which accelerated Pu(III) to be expelled from the host magnetite.[67,68,82,83]

Since Fe(II) concentration and pH used in the recrystallization step are similar to the geochemical settings in the near-field of anoxic deep-underground repositories hosting nuclear waste in steel containers, our recrystallization experiment suggests that structural incorporation of Pu(III) is likely less favorable under such conditions than surface complexation.

ASSOCIATED CONTENT

Supporting Information

The Supporting Information is available free of charge on the ACS Publications website at DOI: 10.1021/acsearthspacechem.9b00147.

LSC and XPS data and additional EXAFS shell fits of sample Pu-Mag-1300 (PDF)

AUTHOR INFORMATION

Corresponding Author

*E-mail: scheinost@esrf.fr.

ORCID

Thomas Dumas: 0000-0001-6425-6484

Andreas C. Scheinost: 0000-0002-6608-5428

Notes

The authors declare no competing financial interest.

ACKNOWLEDGMENTS

This project was financially supported by BMBF project 02NUK019D and the European FP7 project TALISMAN (Transnational Access to Large Infrastructure for the Safe MAnagement of Actinides). The wet-chemistry work was performed in the controlled area of KIT-INE with support of KIT-INE technical staff, and the XAFS studies were performed in the controlled area of The Rossendorf Beamline at ESRF (BM20) with support from the ESRF Radioprotection Group.

REFERENCES

(1) Choppin, G. R. Actinide speciation in the environment. *Radiochim. Acta* **2003**, *91*, 645−650.

(2) Kaplan, D. I.; Demirkanli, D. I.; Gumapas, L.; Powell, B. A.; Fjeld, R. A.; Molz, F. J.; Serkiz, S. M. Eleven-year field study of Pu migration from PuIII, IV, and VI sources. *Environ. Sci. Technol.* **2006**, *40* (2), 443−448.

(3) Kaplan, D. I.; Powell, B. A.; Demirkanli, D. I.; Fjeld, R. A.; Molz, F. J.; Serkiz, S. M.; Coates, J. T. Influence of oxidation states on plutonium mobility during long-term transport through an unsaturated subsurface environment. *Environ. Sci. Technol.* **2004**, *38* (19), 5053−5058.

(4) Kaplan, D. I.; Powell, B. A.; Gumapas, L.; Coates, J. T.; Fjeld, R. A.; Diprete, D. P. Influence of pH on plutonium desorption/solubilization from sediment. *Environ. Sci. Technol.* **2006**, *40* (19), 5937−5942.

(5) Duff, M. C.; Newville, M.; Hunter, D. B.; Bertsch, P. M.; Sutton, S. R.; Triay, I. R.; Vaniman, D. T.; Eng, P.; Rivers, M. L. Micro-XAS studies with sorbed plutonium on tuff. *J. Synchrotron Radiat.* **1999**, *6*, 350−352.

(6) Kersting, A. B.; Efurd, D. W.; Finnegan, D. L.; Rokop, D. J.; Smith, D. K.; Thompson, J. L. Migration of plutonium in ground water at the Nevada Test Site. *Nature* **1999**, *397*, 56−59.

(7) Novikov, A. P.; Kalmykov, S. N.; Utsunomiya, S.; Ewing, R. C.; Horreard, F.; Merkulov, A.; Clark, S. B.; Tkachev, V. V.; Myasoedov, B. F. Colloid transport of plutonium in the far-field of the Mayak Production Association, Russia. *Science* **2006**, *314*, 638−641.

(8) Jeanson, A.; Berthon, C.; Coantic, S.; Den Auwer, C.; Floquet, N.; Funke, H.; Guillaneux, D.; Hennig, C.; Martinez, J.; Moisy, P.; Petit, S.; Proux, O.; Quemeneur, E.; Solari, P. L.; Subra, G. The role

DOI: 10.1021/acsearthspacechem.9b00147
ACS Earth Space Chem. 2019, 3, 2197−2206

of aspartyl-rich pentapeptides in comparative complexation of actinide(IV) and iron(III). Part 1. *New J. Chem.* **2009**, *33* (5), 976−985.
(9) Jeanson, A.; Ferrand, M.; Funke, H.; Hennig, C.; Moisy, P.; Solari, P. L.; Vidaud, C.; Den Auwer, C. The Role of Transferrin in Actinide(IV) Uptake: Comparison with Iron(III). *Chem. - Eur. J.* **2010**, *16* (4), 1378−1387.
(10) Marquardt, C. M.; Seibert, A.; Artinger, R.; Denecke, M. A.; Kuczewski, B.; Schild, D.; Fanghanel, T. The redox behaviour of plutonium in humic rich groundwater. *Radiochim. Acta* **2004**, *92* (9−11), 617−623.
(11) Moll, H.; Merroun, M. L.; Hennig, C.; Rossberg, A.; Selenska-Pobell, S.; Bernhard, G. The interaction of Desulfovibrio äspöensis DSM 10631T with plutonium. *Radiochim. Acta* **2006**, *94*, 815−824.
(12) Neu, M. P.; Icopini, G. A.; Boukhalfa, H. Plutonium speciation affected by environmental bacteria. *Radiochim. Acta* **2005**, *93* (11), 705−714.
(13) Schmeide, K.; Reich, T.; Sachs, S.; Bernhard, G. Plutonium(III) complexation by humic substances studied by X-ray absorption fine structure spectroscopy. *Inorg. Chim. Acta* **2006**, *359* (1), 237−242.
(14) Sanchez, A. L.; Murray, J. W.; Sibley, T. H. The adsorption of plutonium IV and V on goethite. *Geochim. Cosmochim. Acta* **1985**, *49* (11), 2297−2307.
(15) Metz, V.; Geckeis, H.; Gonzalez-Robles, E.; Loida, A.; Bube, C.; Kienzler, B. Radionuclide behaviour in the near-field of a geological repository for spent nuclear fuel. *Radiochim. Acta* **2012**, *100* (8−9), 699−713.
(16) Schlegel, M. L.; Bataillon, C.; Blanc, C.; Pret, D.; Foy, E. Anodic activation of iron corrosion in clay media under water-saturated conditions at 90 degrees C: Characterization of the corrosion interface. *Environ. Sci. Technol.* **2010**, *44* (4), 1503−1508.
(17) Wersin, P.; Jenni, A.; Mader, U. K. Interaction of corroding iron with bentonite in the ABM1 experiment at Aspo, Sweden: A microscopic approach. *Clays Clay Miner.* **2015**, *63* (1−2), 51−68.
(18) Grambow, B.; Smailos, E.; Geckeis, H.; Muller, R.; Hentschel, H. Sorption and reduction of uranium(VI) on iron corrosion products under reducing saline conditions. *Radiochim. Acta* **1996**, *74*, 149−154.
(19) El Hajj, H.; Abdelouas, A.; El Mendili, Y.; Karakurt, G.; Grambow, B.; Martin, C. Corrosion of carbon steel under sequential aerobic-anaerobic environmental conditions. *Corros. Sci.* **2013**, *76*, 432−440.
(20) Singer, D. M.; Chatman, S. M.; Ilton, E. S.; Rosso, K. M.; Banfield, J. F.; Waychunas, G. A. U(VI) Sorption and Reduction Kinetics on the Magnetite (111) Surface. *Environ. Sci. Technol.* **2012**, *46* (7), 3821−3830.
(21) Singer, D. M.; Chatman, S. M.; Ilton, E. S.; Rosso, K. M.; Banfield, J. F.; Waychunas, G. A. Identification of Simultaneous U(VI) Sorption Complexes and U(IV) Nanoprecipitates on the Magnetite (111) Surface. *Environ. Sci. Technol.* **2012**, *46* (7), 3811−3820.
(22) Cevirim-Papaioannou, N.; Yalcintas, E.; Gaona, X.; Dardenne, K.; Altmaier, M.; Geckeis, H. Redox chemistry of uranium in reducing, dilute to concentrated NaCl solutions. *Appl. Geochem.* **2018**, *98*, 286−300.
(23) Bruno, J.; González-Siso, M. R.; Duro, L.; Gaona, X.; Altmaier, M. Key master variables affecting the mobility of Ni, Pu, Tc and U in the near field of the SFR repository. *SKB report TR-18−01* **2018**, 79.
(24) Latta, D. E.; Gorski, C. A.; Boyanov, M. I.; O'Loughlin, E. J.; Kemner, K. M.; Scherer, M. M. Influence of Magnetite Stoichiometry on U-VI Reduction. *Environ. Sci. Technol.* **2012**, *46* (2), 778−786.
(25) Scheinost, A. C.; Steudtner, R.; Hübner, R.; Weiss, S.; Bok, F. Neptunium^{V} retention by siderite under anoxic conditions: Precipitation of NpO_2−like nanoparticles and of Np^{IV} pentacarbonate. *Environ. Sci. Technol.* **2016**, *50*, 10413−10420.
(26) Nakata, K.; Nagasaki, S.; Tanaka, S.; Sakamoto, Y.; Tanaka, T.; Ogawa, H. Reduction rate of neptunium(V) in heterogeneous solution with magnetite. *Radiochim. Acta* **2004**, *92* (3), 145−149.
(27) Fellhauer, D. Untersuchungen zur Redoxchemie und Löslichkeit von Neptunium und Plutonium. PhD thesis, University of Heidelberg, Germany, 2013.
(28) Charlet, L.; Scheinost, A. C.; Tournassat, C.; Greneche, J. M.; Géhin, A.; Fernández-Martínez, A.; Coudert, S.; Tisserand, D.; Brendle, J. Electron transfer at the mineral/water interface: Selenium reduction by ferrous iron sorbed on clay. *Geochim. Cosmochim. Acta* **2007**, *71*, 5731−5749.
(29) Scheinost, A. C.; Charlet, L. Selenite reduction by mackinawite, magnetite and siderite: XAS characterization of nanosized redox products. *Environ. Sci. Technol.* **2008**, *42* (6), 1984−1989.
(30) Scheinost, A. C.; Kirsch, R.; Banerjee, D.; Fernandez-Martinez, A.; Zaenker, H.; Funke, H.; Charlet, L. X-ray absorption and photoelectron spectroscopy investigation of selenite reduction by FeII-bearing minerals. *J. Contam. Hydrol.* **2008**, *102*, 228−245.
(31) Kobayashi, T.; Scheinost, A. C.; Fellhauer, D.; Gaona, X.; Altmaier, M. Redox behavior of Tc(VII)/Tc(IV) under various reducing conditions in 0.1 M NaCl solutions. *Radiochim. Acta* **2013**, *101* (5), 323−332.
(32) Yalçıntaş, E.; Scheinost, A. C.; Gaona, X.; Altmaier, M. Systematic XAS study on the reduction and uptake of Tc by magnetite and mackinawite. *Dalton Trans* **2016**, *45*, 17874−17885.
(33) Powell, B. A.; Fjeld, R. A.; Kaplan, D. I.; Coates, J. T.; Serkiz, S. M. $Pu(V)O_2^+$ adsorption and reduction by synthetic magnetite (Fe_3O_4). *Environ. Sci. Technol.* **2004**, *38* (22), 6016−6024.
(34) Powell, B. A.; Fjeld, R. A.; Kaplan, D. I.; Coates, J. T.; Serkiz, S. M. $Pu(V)O_2^+$ adsorption and reduction by synthetic hematite and goethite. *Environ. Sci. Technol.* **2005**, *39* (7), 2107−2114.
(35) Romanchuk, A. Y.; Kalmykov, S. N.; Aliev, R. A. Plutonium sorption onto hematite colloids at femto- and nanomolar concentrations. *Radiochim. Acta* **2011**, *99* (3), 137−144.
(36) Kirsch, R.; Fellhauer, D.; Altmaier, M.; Neck, V.; Rossberg, A.; Fanghänel, T.; Charlet, L.; Scheinost, A. C. Oxidation state and local structure of plutonium reacted with magnetite, mackinawite and chukanovite. *Environ. Sci. Technol.* **2011**, *45* (17), 7267−7274.
(37) Shannon, R. D. Revised effective ionic radii and systematic studies of interatomic distances in halides and chalcogenides. *Acta Crystallogr., Sect. A: Cryst. Phys., Diffr., Theor. Gen. Crystallogr.* **1976**, *32* (SEP1), 751−767.
(38) Dulnee, S.; Banerjee, D.; Merkel, B. J.; Scheinost, A. C. Surface complexation and oxidation of Sn^{II} by nanomagnetite. *Environ. Sci. Technol.* **2013**, *47* (22), 12852−12859.
(39) Stewart, B. D.; Nico, P. S.; Fendorf, S. Stability of Uranium Incorporated into Fe (Hydr)oxides under Fluctuating Redox Conditions. *Environ. Sci. Technol.* **2009**, *43* (13), 4922−4927.
(40) Nico, P. S.; Stewart, B. D.; Fendorf, S. Incorporation of Oxidized Uranium into Fe (Hydr)oxides during Fe(II) Catalyzed Remineralization. *Environ. Sci. Technol.* **2009**, *43* (19), 7391−7396.
(41) Pidchenko, I.; Kvashnina, K. O.; Yokosawa, T.; Finck, N.; Bahl, S.; Schild, D.; Polly, R.; Bohnert, E.; Rossberg, A.; Gottlicher, J.; Dardenne, K.; Rothe, J.; Schafer, T.; Geckeis, H.; Vitova, T. Uranium Redox Transformations after U(VI) Coprecipitation with Magnetite Nanoparticles. *Environ. Sci. Technol.* **2017**, *51* (4), 2217−2225.
(42) De Silva, C. R.; Smith, S.; Shim, I.; Pyun, J.; Gutu, T.; Jiao, J.; Zheng, Z. P. Lanthanide(III)-doped magnetite nanoparticles. *J. Am. Chem. Soc.* **2009**, *131* (18), 6336.
(43) Moon, J. W.; Roh, Y.; Yeary, L. W.; Lauf, R. J.; Rawn, C. J.; Love, L. J.; Phelps, T. J. Microbial formation of lanthanide-substituted magnetites by Thermoanaerobacter sp TOR-39. *Extremophiles* **2007**, *11* (6), 859−867.
(44) Kahn, M. L.; Zhang, Z. J. Synthesis and magnetic properties of CoFe2O4 spinel ferrite nanoparticles doped with lanthanide ions. *Appl. Phys. Lett.* **2001**, *78* (23), 3651−3653.
(45) Drake, P.; Cho, H. J.; Shih, P. S.; Kao, C. H.; Lee, K. F.; Kuo, C. H.; Lin, X. Z.; Lin, Y. J. Gd-doped iron-oxide nanoparticles for tumour therapy via magnetic field hyperthermia. *J. Mater. Chem.* **2007**, *17* (46), 4914−4918.

DOI: 10.1021/acsearthspacechem.9b00147
ACS Earth Space Chem. 2019, 3, 2197−2206

(46) Sattar, A. A.; ElShokrofy, K. M. Rare earth doping effect on the electrical properties of Cu-Zn ferrites. *J. Phys. IV* **1997**, *7* (C1), 245−246.
(47) Zhang, H. H.; Malik, V.; Mallapragada, S.; Akinc, M. Synthesis and characterization of Gd-doped magnetite nanoparticles. *J. Magn. Magn. Mater.* **2017**, *423*, 386−394.
(48) Park, J. C.; Yeo, S.; Kim, M.; Lee, G. T.; Seo, J. H. Synthesis and characterization of novel lanthanide-doped magnetite@Au core@shell nanoparticles. *Mater. Lett.* **2016**, *181*, 272−277.
(49) Soldatov, M. A.; Göttlicher, J.; Kubrin, S. P.; Guda, A. A.; Lastovina, A.; Bugaev, A. L.; Rusalev, Y. V.; Soldatov, A. V.; Lamberti, C. Insight from X-ray absorption spectroscopy to octahedral/tetrahedral site distribution in Sm-doped iron oxide magnetic nanoparticles. *J. Phys. Chem. C* **2018**, *122*, 8543−8552.
(50) Finck, N.; Nedel, S.; Dideriksen, K.; Schlegel, M. L. Trivalent actinide uptake by iron (hydr)oxides. *Environ. Sci. Technol.* **2016**, *50* (19), 10428−10436.
(51) Frierdich, A. J.; McBride, A.; Tompkins, S.; Southall, S. C. Nickel cycling and negative feedback on Fe(II)-catalyzed recrystallization of goethite. *ACS Earth Space Chem.* **2019**, DOI: 10.1021/acsearthspacechem.9b00137.
(52) Boland, D. D.; Collins, R. N.; Payne, T. E.; Waite, T. D. Effect of Amorphous Fe(III) Oxide Transformation on the Fe(II)-Mediated Reduction of U(VI). *Environ. Sci. Technol.* **2011**, *45* (4), 1327−1333.
(53) Catalano, J. G.; Fenter, P.; Park, C.; Rosso, K. M.; Frierdich, A. J.; Otemuyiwa, B. T. Fe(II)-induced structural transformations of hematite surfaces and their impact on contaminants. *Geochim. Cosmochim. Acta* **2010**, *74* (12), A150.
(54) Handler, R. M.; Beard, B. L.; Johnson, C. M.; Scherer, M. M. Atom Exchange between Aqueous Fe(II) and Goethite: An Fe Isotope Tracer Study. *Environ. Sci. Technol.* **2009**, *43* (4), 1102−1107.
(55) Pedersen, H. D.; Postma, D.; Jakobsen, R.; Larsen, O. Fast transformation of iron oxyhydroxides by the catalytic action of aqueous Fe(II). *Geochim. Cosmochim. Acta* **2005**, *69* (16), 3967−3977.
(56) Jones, A. M.; Collins, R. N.; Rose, J.; Waite, T. D. The effect of silica and natural organic matter on the Fe(II)-catalysed transformation and reactivity of Fe(III) minerals. *Geochim. Cosmochim. Acta* **2009**, *73* (15), 4409−4422.
(57) Wan, J.; Cai, W.; Meng, X.; Liu, E. Monodisperse water-soluble magnetite nanoparticles prepared by polyol process for high-performance magnetic resonance imaging. *Chem. Commun.* **2007**, No. 47, 5004−5006.
(58) Wang, J.; Deng, T.; Dai, Y. J. Study on the processes and mechanism of the formation of Fe3O4 at low temperature. *J. Alloys Compd.* **2005**, *390* (1−2), 127−132.
(59) Viollier, E.; Inglett, P. W.; Hunter, K.; Roychoudhury, A. N.; Van Cappellen, P. The ferrozine method revisited: Fe(II)/Fe(III) determination in natural waters. *Appl. Geochem.* **2000**, *15* (6), 785−790.
(60) Wright, J. P.; Attfield, J. P.; Radaelli, P. G. Charge ordered structure of magnetite Fe3O4 below the Verwey transition. *Phys. Rev. B: Condens. Matter Mater. Phys.* **2002**, *66* (21), 214422.
(61) Chtoun, E. H.; Hanebali, L.; Garnier, P. X-ray Rietveld analysis of (1-x)$A_2Ti_2O_7$ xFe_2TiO_5 (A= Eu,Y) solid solutions. *Ann. Chim.* **2001**, *26* (3), 27−32.
(62) Seah, M. P.; Gilmore, L. S.; Beamson, G. XPS: Binding energy calibration of electron spectrometers 5 - Re-evaluation of the reference energies. *Surf. Interface Anal.* **1998**, *26* (9), 642−649.
(63) Webb, S. M. Sixpack: a graphical user interface for XAS analysis using IFEFFIT. *Phys. Scr.* **2005**, *T115*, 1011−1014.
(64) Ressler, T. WinXAS: a program for X-ray absorption spectroscopy data analysis under MS-Windows. *J. Synchrotron Radiat.* **1998**, *5* (2), 118−122.
(65) Ankudinov, A. L.; Rehr, J. J. Relativistic calculations of spin-dependent x-ray-absorption spectra. *Phys. Rev. B: Condens. Matter Mater. Phys.* **1997**, *56*, 1712−1728.
(66) Rossberg, A.; Reich, T.; Bernhard, G. Complexation of uranium(VI) with protocatechuic acid - application of iterative transformation factor analysis to EXAFS spectroscopy. *Anal. Bioanal. Chem.* **2003**, *376* (5), 631−638.
(67) Cho, H.-R.; Youn, Y.-S.; Jung, E. C.; Cha, W. Hydrolysis of trivalent plutonium and solubility of Pu(OH)(3) (am) under electrolytic reducing conditions. *Dalton Transactions* **2016**, *45* (48), 19449−19457.
(68) Tasi, A.; Gaona, X.; Fellhauer, D.; Boettle, M.; Rothe, J.; Dardenne, K.; Schild, D.; Grive, M.; Colas, E.; Bruno, J.; Kallstrom, K.; Altmaier, M.; Geckeis, H. Redox behavior and solubility of plutonium under alkaline, reducing conditions. *Radiochim. Acta* **2018**, *106* (4), 259−279.
(69) Dalodière, E.; Virot, M.; Dumas, T.; Guillaumont, D.; Illy, M.-C.; Berthon, C.; Guerin, L.; Rossberg, A.; Venault, L.; Moisy, P.; Nikitenko, S. I. Structural and magnetic susceptibility characterization of Pu(V) aqua ion using sonochemistry as a facile synthesis method. *Inorg. Chem. Front.* **2018**, *5*, 100−111.
(70) Funke, H.; Scheinost, A. C.; Chukalina, M. Wavelet analysis of extended X-ray absorption fine structure data. *Phys. Rev. B: Condens. Matter Mater. Phys.* **2005**, *B 71*, 094110.
(71) Chikalla, T. D.; McNeilly, C. E.; Skavdahl, R. E. The plutonium-oxygen system. *J. Nucl. Mater.* **1964**, *12* (2), 131−141.
(72) Marques Fernandes, M.; Scheinost, A.C.; Baeyens, B. Sorption of trivalent lanthanides and actinides onto montmorillonite: Macroscopic, thermodynamic and structural evidence for ternary hydroxo and carbonato surface complexes on multiple sorption sites. *Water Res.* **2016**, *99*, 74−82.
(73) Daniels, L. M. W. Structures and Properties of Perovskites and Pyrochlores from Hydrothermal Synthesis. PhD thesis, University of Warwick, 2015.
(74) Belin, R. C.; Martin, P. M.; Valenza, P. J.; Scheinost, A. C. Experimental insight into the radiation resistance of zirconia-based americium ceramics. *Inorg. Chem.* **2009**, *48*, 5376−5381.
(75) Bender, W. M.; Becker, U. Quantum-mechanical investigation of the structures and energetics of uranium and plutonium incorporated into the magnetite (Fe_3O_4 lattice. *ACS Earth Space Chem.* **2019**, *3*, 637−651.
(76) Um, W.; Chang, H. S.; Icenhower, J. P.; Lukens, W. W.; Serne, R. J.; Qafoku, N. P.; Westsik, J. H.; Buck, E. C.; Smith, S. C. Immobilization of 99-Technetium (VII) by Fe(II)-Goethite and Limited Reoxidation. *Environ. Sci. Technol.* **2011**, *45* (11), 4904−4913.
(77) Marshall, T. A.; Morris, K.; Law, G. T. W.; Mosselmans, J. F. W.; Bots, P.; Parry, S. A.; Shaw, S. Incorporation and Retention of 99-Tc(IV) in Magnetite under High pH Conditions. *Environ. Sci. Technol.* **2014**, *48* (20), 11853−11862.
(78) Rajendran, M.; Bhattacharya, A. K. Nanocrystalline orthoferrite powders: Synthesis and magnetic properties. *J. Eur. Ceram. Soc.* **2006**, *26* (16), 3675−3679.
(79) Lumpkin, G. R.; Ewing, R. C. Alpha-decay damage in minerals of the pyrochlore group. *Phys. Chem. Miner.* **1988**, *16* (1), 2−20.
(80) Wang, S. X.; Begg, B. D.; Wang, L. M.; Ewing, R. C.; Weber, W. J.; Kutty, K. V. G. Radiation stability of gadolinium zirconate: A waste form for plutonium disposition. *J. Mater. Res.* **1999**, *14* (12), 4470−4473.
(81) Sellin, P.; Leupin, O. X. The use of clay as an engineered barrier in radioactive waste management - A review. *Clays Clay Miner.* **2013**, *61* (6), 477−498.
(82) Watson, E. B. A conceptual model for near-surface kinetic controls on the trace-element and stable isotope composition of abiogenic calcite crystals. *Geochim. Cosmochim. Acta* **2004**, *68* (7), 1473−1488.
(83) Thien, B. M. J.; Kulik, D. A.; Curti, E. Modeling trace element uptake kinetics in secondary minerals. In *Proceedings of the Fourteenth International Symposium on Water-Rock Interaction, WRI 14*, Hellmann, R., Pitsch, H., Eds.; Elsevier Science: Amsterdam, 2013; Vol. 7, pp 838−841.

DOI: 10.1021/acsearthspacechem.9b00147
ACS Earth Space Chem. 2019, 3, 2197−2206

NOTE ADDED AFTER ASAP PUBLICATION

This paper was published ASAP on August 6, 2019, with a missing reference in the Introduction. The corrected version was reposted on August 19, 2019.

DOI: 10.1021/acsearthspacechem.9b00147
ACS Earth Space Chem. 2019, 3, 2197−2206